Journal of Materials Chemistry A

ROYAL SOCIETY OF CHEMISTRY

PAPER

View Article Online
View Journal

Cite this: DOI: 10.1039/d5ta10078j

Stabilization of planar heterojunction solar cells using a dimethyl sulfoxide treated hole transport layer

Elaheh Habibzadeh, Joseph Palathinkal Thomas and Kam Tong Leung *

Heterojunction solar cells (HSCs) have gained attention in the field of renewable energy for their potential to combine the benefits of both crystalline silicon and thin-film technologies, thus offering high efficiency and relatively low manufacturing cost. However, several challenges, particularly those related to long-term stability and performance degradation, need to be addressed for commercial scalability. Resolving the durability issue requires innovative strategies through modification of key components such as the hole transport layer (HTL). This study investigates the stabilization of HSCs by addition of dimethyl sulfoxide (DMSO) to poly(3,4ethylenedioxythiophene)-poly(styrenesulfonate) (PEDOT:PSS) solutions modified with and without other cosolvents. Known for their cost-effectiveness and high efficiency, HSCs have been found to benefit significantly from the addition of DMSO to PEDOT:PSS. Our results show that the addition of DMSO to ethylene glycol and methanol (EM) modified PEDOT:PSS solution increases the electrical conductivity and greatly improves the stability of the fabricated solar cells by enhancing phase separation and reducing charge recombination. The sample prepared with a 3 wt% DMSO concentration in EM is found to exhibit the best performance in stability, retaining 89.4% of its initial efficiency after 72 h of ambient storage upon fabrication, in contrast to the control sample that loses half of its efficiency in the same duration, all without the use of any protective encapsulation. This work highlights the potential of DMSO in enhancing the durability and effectiveness of EM modified PEDOT:PSS-based solar cells, making DMSO-EM a promising cosolvent mixture for fabricating high-efficiency and intrinsically stable HSCs in the green energy evolution.

Received 9th December 2025
Accepted 6th April 2026

DOI: 10.1039/d5ta10078j

rsc.li/materials-a

Introduction

Heterojunction solar cells (HSCs) have the benefit of combining the advantages of both organic and inorganic groups of materials.[1] The low cost and flexibility of the fabrication process, easy processibility using simple solutions with a high degree of tunability, and great potential for achieving high efficiencies have made HSCs promising devices for green energy generation.[2] The incorporation of highly conductive and transparent organic polymers by spin-coating makes the treatment of the hole transport layer (HTL) of HSCs much simpler.[3] One of the most popular p-type organic polymers that has been used extensively as the HTL in solution-processed solar cells is poly(3,4ethylenedioxythiophene)-poly(styrenesulfonate) or PEDOT:PSS. Not only is a thin film of PEDOT:PSS highly transparent in the visible light (400–800 nm) region, but its high electrical conductivity of 10^{-2} to 10^{3} S cm^{-1} achievable by simply adding cosolvents also makes a PEDOT:PSS film highly desirable in advanced electronic devices including solar cells.[4] The existing ionic interaction between the positively charged conjugated PEDOT and the water-soluble PSS with a negative charge results in a homogeneous and conductive polymer blend.[5] The conductivity of the film formed by spin-coating a PEDOT:PSS aqueous solution has been found to strongly depend on the amount of PEDOT in the core relative to that of PSS in the shell.[6] Therefore, the majority of the treatment methods, including doping, solution post-processing, and bilayer treatment, have focused on increasing the ratio of the conductive PEDOT core to the insulating hydrophilic PSS shell.[7]

The addition of cosolvents to PEDOT:PSS before the coating step or through post-treatment methods has been found to enhance the conductivity of the polymer. These treatments generally cause a reduction of the coulombic interaction between PEDOT and PSS that transforms the spherical morphology of the grains into a more ellipsoidal shape to facilitate better charge transfer while removing the insulating hygroscopic PSS from the surface.[8–14] The solution processability of PEDOT:PSS with different cosolvents such as dimethylsulfoxide (DMSO), ethylene glycol (EG), and methanol has been found to enhance the electrical conductivity through reconstruction of the PEDOT domains in the PSS matrix.[15–21] These methods mainly affect the quality of the as-formed films in terms of morphology and crystallinity, aggregation and film

WATLab and Department of Chemistry, University of Waterloo, Waterloo, Ontario, N2L 3G1, Canada. E-mail: tong@uwaterloo.ca

adhesion, surface passivation, charge carrier mobility, and light absorption.[6] Despite its many advantages, PEDOT:PSS is prone to degradation upon prolonged exposure to ambient conditions because of its acidic and hygroscopic nature, which leads to a decrease in the overall performance and stability of the solar cells.[22,23] Previous efforts to improve the stability of PEDOT:PSS have largely focused on mitigating the effects of its acidic and hygroscopic PSS component through strategies such as chemical crosslinking, pH modification, solvent or post-treatment engineering, and device-level encapsulation.[23–29] While these approaches can reduce moisture sensitivity or enhance conductivity, they often require additional processing steps and they primarily target electrical performance rather than intrinsic stability. In contrast, the present work demonstrates that introducing a small, optimized amount of DMSO into an EG–methanol modified PEDOT:PSS formulation enables both high efficiency (13.4%) and improved ambient stability without encapsulation in a simple planar Si heterojunction structure. This represents a process-minimal, solution-level approach that directly enhances intrinsic durability, distinguishing it from prior stabilization strategies. DMSO has been reported to facilitate better dispersion of PSS, resulting in a more homogeneous film and thereby leading to an increased charge carrier mobility and reduced charge recombination.[30] The addition of mixed cosolvents of methanol and EG has also been found to improve the performance of solar cells that were made with modified PEDOT:PSS.[15] Here, we investigate the impact of adding DMSO to the PEDOT:PSS solution containing methanol and EG on the longevity of HSCs. The stability of HSCs after fabrication is an under-explored area that could offer new perspectives on developing more durable solar cells. Most stability studies have focused on introducing techniques involving encapsulation of already fabricated solar cells rather than making more stable solar cells without further modification. There is therefore an acute need to develop intrinsically stable solar cells to lower the cost of production and to further reduce the complexity of the process. We show that HSCs fabricated with our DMSO added, cosolvent-modified PEDOT:PSS solutions require no additional post-fabrication step for markedly reducing degradation while being kept under ambient conditions over an extended duration.

Experimental

Co-solvent modification of PEDOT:PSS

Highly conducting grade PEDOT:PSS (PH1000) was purchased from Clevios and filtered by using a 0.45 μm polyvinylidene fluoride syringe filter to remove any fine particles prior to use. All the other chemicals were obtained from commercial sources and were used as purchased. The control cosolvent solution of PEDOT:PSS (denoted here as EM) contained 8 wt% ethylene glycol (EG) and 8 wt% methanol, with PEDOT:PSS making up the remaining solution. Three cosolvent solutions containing DMSO as an additional cosolvent were prepared with selected DMSO concentrations of 1 wt% (designated here as EMD1), 3 wt% (EMD3) and 5 wt% (EMD5) added to the control cosolvent solution of PEDOT:PSS (EM). A 0.25 wt% FS-300 surfactant has been premixed into the EM and EMD cosolvent solutions prior to the spin-coating process.

Solar cell fabrication

Single-side polished phosphorus-doped n-type silicon (100) wafers (Virginia Semiconductor Inc.) with a thickness of 280 ± 25 μm and a resistivity of 0.04–0.07 Ω cm were cut into 10 × 10 mm^2 chips. These Si chips were ultrasonicated in acetone and then in isopropyl alcohol (IPA) for 10 min each, and they were also rinsed with ultrapure water (with a resistivity of 18.2 MΩ cm at 21.6 °C) after each round of sonication. The Si chips were then immersed in 5% HF for 2 min to remove the native oxides from the surface followed by rinsing with ultrapure water and drying under a nitrogen stream. A dual target magnetron sputtering system (EMS 575X) was used to deposit a 200 nm thick film of aluminum on the unpolished side of a Si chip to serve as the bottom electrode. The Si chip was then allowed to grow a layer of silicon oxide on the surface of its polished side for 20 min under ambient conditions. Optimization of the thickness of the as-grown oxide layer has been discussed in our previous work.[31] PEDOT:PSS solutions prepared with different cosolvents (EM, EMD1, EMD3 and EMD5) were spin-coated on the Si substrates at a rate of 4000 rpm for 1 min. The resulting PEDOT:PSS coated Si substrates were then baked for 10 min on a hotplate at 110 °C in air, before deposition of a 50 nm thick Ag film by magnetron sputtering through a comb-like busbar shadow mask to serve as the top electrode of the solar cell. A schematic structure of a typical HSC is shown in Fig. 1.

To prepare the films for sheet resistance and conductivity measurement, 1 × 1 cm^2 glass substrates were sonicated in ultrapure water containing Alconox detergent for 10 min, followed by 10 min sonication each in ultrapure water, acetone and IPA. EM and EMD films were then spin-coated onto these substrates and baked under the same conditions used for the polymer coating in the solar cell process. The sheet resistance and conductivity of the EM and EMD films were measured in a Van der Pauw configuration by using a Hall effect measurement system (Ecopia HMS-5300). A UV-vis-NIR spectrophotometer (PerkinElmer Lambda 1050) was used to collect the reflectance spectra of the film samples. X-ray photoelectron spectroscopy (XPS) studies were conducted in a Thermo Scientific Nexsa G2 system, employing a monochromatic Al Kα source (1486.6 eV photon energy). CasaXPS software was used for peak fitting of characteristic photopeak features with appropriate subtraction of the Shirley background. The topography and

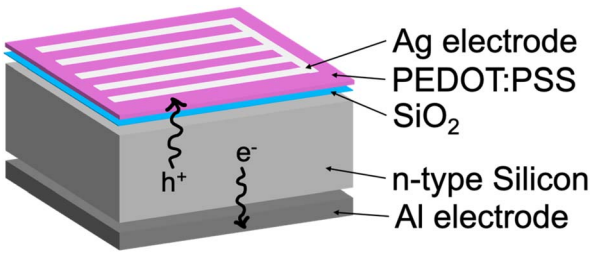

Fig. 1 Illustration of the device structure of a heterojunction solar cell.

surface roughness were examined by using tapping-mode atomic force microscopy (AFM) in an Asylum Cypher system. Samples for both XPS and AFM were prepared on silicon substrates, using the same fabrication procedure employed in solar cell fabrication.

Characterization

The solar cell performance was characterized by using current density *vs.* voltage (*J–V*) and external quantum efficiency (EQE) measurements in PV Measurements IV5 and QEX10 systems, respectively. The *J–V* characteristics were obtained under an illumination intensity of 100 mW cm^{-2} (1 Sun), using a class ABA solar simulator equipped with an AM1.5 G filter. In order to calibrate the intensity of the light source, a Si reference cell (PVM782 with a BK7 window) was used before performing any measurements. During the *J–V* measurements, an illuminated device area of 8.4 × 8.4 mm^2 was defined. The EQE measurements were carried out under monochromatic light, obtained by using a dual-grating monochromator with a xenon arc lamp, along with a germanium photodiode detector. The typical area illuminated for EQE measurements was approximately 1 × 3.5 mm^2.

Results and discussion

To investigate the effect of DMSO on the performance of HSCs, EM solutions containing additional selected amounts of DMSO were used to fabricate solar cells. After fabrication, the devices were stored in small boxes (to keep them dust-free) under laboratory ambient conditions, specifically, at 1 atm, 20–23 °C, and 30–50% relative humidity. No glove-box processing, vacuum storage or encapsulation was used. The solar cell performance data of HSCs fabricated using EM solution (*i.e.*, without DMSO) are also collected for reference. Fig. 2a shows the current density *vs.* voltage (*J–V*) curves of the as-fabricated EM, EMD1, EMD3 and EMD5 cells. Evidently, there is significant improvement in the *J–V* curve for the EMD3 cell relative to the EM cell, while the *J–V* curve for EMD1 is similar to that of EM and that for EMD5 appears considerably worse than both EM and EMD1. The solar cell performance parameters of EMD1, EMD3, EMD5, and EM cells are compared in Table S1 (SI). The EMD3 cell is found to exhibit the best result, with a short-circuit current density (J_{SC}) of 30.1 mA cm^{-2}, open-circuit voltage (V_{OC}) of 642.4 mV, fill factor (FF) of 69.4% and power conversion efficiency (PCE) of 13.4%. Fig. 2b compares the *J–V* curves of the EMD3 cell as-fabricated (*i.e.*, with 0 h of ambient storage) and over an extended period of ambient storage time, up to 216 h, and those of EM cells as-fabricated and after 48 h and 72 h of ambient storage. Fig. 2c presents the storage stability trends of solar cell performance metrics of the EMD3 and EM devices obtained from their respective *J–V* curves (Fig. 2b). These solar cell performance data are also summarized in Table S2 (SI). While EMD3 retains relatively stable J_{SC}, V_{OC}, FF, and PCE over time, EM shows a considerable decline in all except J_{SC} parameters, indicating poor stability. For example, the PCE for EMD3 (13.4%) is found to be remarkably stable, with

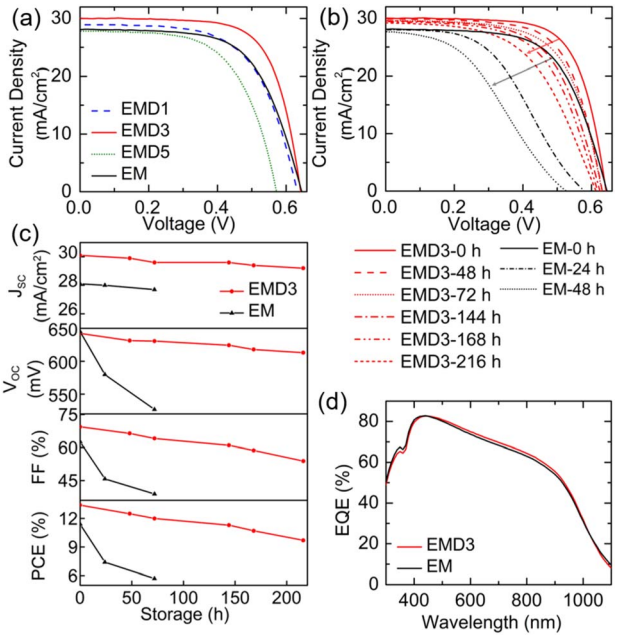

Fig. 2 (a) Current density–voltage (*J–V*) curves for as-fabricated EM, EMD1, EMD3, and EMD5 solar cell samples. (b) *J–V* curves of EMD3 after 0 h, 48 h, 72 h, 144 h, 168 h and 216 h of ambient storage and of EM after 0 h, 24 h, and 72 h of ambient storage. Arrows indicate the direction of performance evolution during ambient ageing for EM (black) and EMD3 (red) devices. (c) Solar cell performance parameters (J_{SC}, V_{OC}, FF, and PCE) as functions of ambient storage time for EMD3 and EM cells. (d) Corresponding EQE spectra of as-fabricated EM and EMD3 solar cells.

a reduction of 10.6% (to 12.0%) after 72 h and 27.9% (to 9.7%) after 216 h of ambient storage. In contrast, the EM cell has a significant 34.4% decrease in PCE from 11.4% to 7.4% in just 24 h (Fig. 2c). Fig. 2d compares the EQE spectra of the EMD3 and EM as-fabricated cells. While the two EQE spectra are found to be nearly the same, the discernibly small difference indicates that the EMD3 cell is slightly higher in light absorption and carrier collection efficiency than the EM cell in the 400–900 nm region. Furthermore, no discernible differences are found in the EQE profiles of EMD3 and EM after 72 h of ambient storage time (not shown), suggesting that EQE data are not very sensitive to degradation changes.

In Table S3 (SI), we show the excellent reproducibility in the similar and consistently high solar cell performance metrics obtained for additional EMD3 cells (that we prepared separately). All the EMD3 cells are also found to remain stable for at least 72 h post-fabrication, and they follow the same degradation trends as shown in Fig. 2c. It should be noted that there is also excellent reproducibility in our fabrication of the reported solar cells. Table S4 (SI) shows the solar cell performance data for the six EMD3 cells separately fabricated on different dates. Three of these cells are used to obtain their degradation trends discussed above and are depicted in Table S3. The spans between the minimum and maximum values are 3.4%, 3.3%, 6.6% and 8.1% of the average values for J_{SC}, V_{OC}, FF and PCE, respectively. Furthermore, the reproducibility of making the

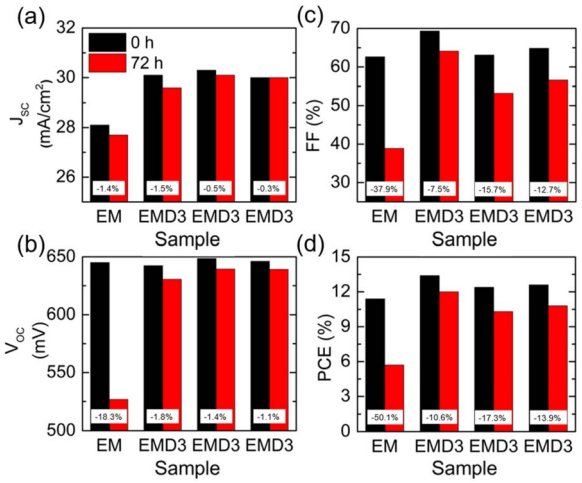

Fig. 3 Solar cell performance parameters (a) J_{SC}, (b) V_{OC}, (c) FF, and (d) PCE of EM and three EMD3 cells as fabricated (black bars) and after 72 h of ambient storage (red bars). The percentage changes after 72 h of ambient storage from the respective as-fabricated values are also indicated.

same measurement at different times for the same cells is illustrated for EMD3 and EM cells in Table S5 (SI). These data are within 0.3%, 0.1%, 0.1% and 0.9% of the average values for J_{SC}, V_{OC}, FF and PCE, respectively.

Fig. 3 and Table S3 compare the degradation of solar cell performance parameters, including J_{SC}, V_{OC}, FF and PCE, after 72 h of ambient storage for the EM and three EMD3 cells. Evidently, the EM cell undergoes significant degradation as its J_{SC}, V_{OC}, FF, and PCE drop by 1.4%, 18.3%, 37.9% and 50.1% from their respective as-fabricated values after 72 h of ambient storage. On the other hand, the EMD3 cells exhibit, on average, a reduction of 0.8% in J_{SC}, 1.4% in V_{OC}, 12.0% in FF and 13.9% in PCE after 72 h of ambient storage. The three best-performing EMD3 devices (#1, #2, and #3 in Table S4) are found to remain highly consistent with one another after 72 hours of ambient storage, with all key performance values staying within the experimental variation. These small variations among the devices highlight the strong reproducibility of the DMSO-modified design. In contrast, the reference solar cell (EM) shows clear degradation over the same period, which confirms the improved stability of the EMD3 cells. These results demonstrate that high efficiency and good reproducibility can potentially be achieved without any post-fabrication treatment (such as encapsulation).

DMSO facilitates the separation of PEDOT from PSS, increasing the connectivity of PEDOT domains and formation of a more robust conductive network.[32] In our study, the addition of DMSO at an optimized wt% to PEDOT:PSS plays a crucial role in the creation of a high-quality film with improved ionic conductivity, charge transport, and mechanical/thermal stability, while preventing rapid degradation due to environmental factors. The partial removal of the insulating and hygroscopic PSS from the surface is another contributing factor that allows DMSO to simultaneously enhance conductivity and make the cell more resilient to degradation over time.[33]

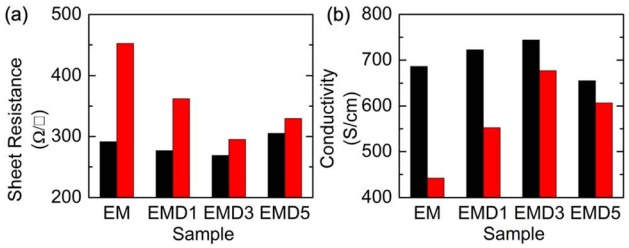

Fig. 4 (a) Sheet resistance and (b) conductivity of EM, EMD1, EMD3 and EMD5 films as-deposited on glass substrates (black) and after 72 h of ambient storage (red).

The sheet resistance (R_S) and conductivity of EM, EMD1, EMD3 and EMD5 films used for fabricating the aforementioned solar cells are measured and they are shown in Fig. 4 to compare the changes in conducting properties and stability before and after 72 h of ambient storage. Among the as-deposited film samples (black bars), EMD1 has a lower R_S (Fig. 4a) and, correspondingly, a slightly higher conductivity than EM (Fig. 4b). The as-deposited EMD3 film has the lowest R_S and the highest conductivity while the as-deposited EMD5 film has the highest R_S and the lowest conductivity, which shows that addition of too much or not enough DMSO can be counter-productive.[16,25,34] After 72 h of ambient storage (red bars), the R_S value of the EM film appears to be more than double, and there is a correspondingly large decrease in the conductivity, which confirms that the EM film is more vulnerable to environmental factors and the degradation process. For the EMD1 film, the changes in R_S and conductivity after 72 h of ambient storage are, respectively, somewhat lower and higher than those of EM but both R_S and conductivity remain considerable, suggesting that the addition of 1 wt% DMSO only has a small impact. For the EMD3 and EMD5 films both with large enough DMSO wt%, there are considerably smaller increases in R_S and corresponding decreases in conductivity (red bars) relative to their respective as-deposited values (black bars), confirming the positive effect of DMSO on reducing the degradation effect on performance upon ambient storage.

Fig. 5a compares the XPS spectra of the S 2p region for the as-deposited EMD3 and EM films (on silicon substrates). The relative composition ratio of PEDOT to PSS components in the samples can be obtained by comparing the intensities (or peak areas) of their respective characteristic S 2p peaks. Evidently, in EMD3 (Fig. 5a1) the S $2p_{3/2}$ ($2p_{1/2}$) peak of PEDOT at 163.7 eV (164.9 eV) binding energy is found to be weaker than that of PSS at 168.1 eV (169.2 eV).[15,35] There is a notable increase in the ratio of PEDOT to PSS in EMD3 (0.452, Fig. 5a1) compared to EM (0.419, Fig. 5a2), which is consistent with the decrease in R_S and the corresponding increase in conductivity of the EMD3 film (arising from the presence of DMSO in PEDOT:PSS), relative to the EM film.

Fig. 5b and c show the corresponding AFM topography and phase images of the EMD3 and EM films, both of which exhibit very similar morphology with ellipsoidal grains. Cosolvents in both samples appear to facilitate elongation of the PEDOT

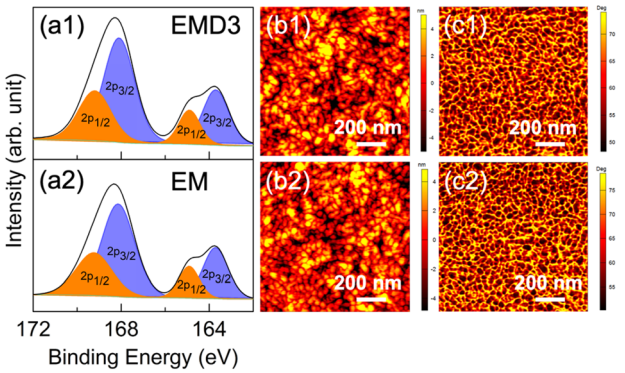

Fig. 5 (a1 and a2) XPS spectra of the S 2p region (left) and AFM images of (b1 and b2) topography (center) and (c1 and c2) phase (right) of EMD3 (a1, b1, and c1) and EM films deposited on silicon substrates (a2, b2, and c2).

chains and thus close packing of grains, which contributes to a smoother charge carrier transfer.[36,37] The root mean square (RMS) roughness of EMD3 is found to be 2.5 nm (Fig. 5b1) while that for EM is 2.3 nm (Fig. 5b2). The slightly rougher surface of the sample with added DMSO (EMD3) shows that enlarged fibrillary structures with aggregated PSS and closely packed PEDOT have a more oriented morphology.[36] While a smoother surface might be preferred for providing better interfacial contacts, a moderate level of roughness could increase light absorption, which may account for the observed EQE enhancement across the 400–900 nm range.[31,38] The reflectance spectra of the silicon substrate and the EM, EMD1, EMD3, and EMD5 films (deposited on silicon substrates) are shown in Fig. S1. With the exception of the Si substrate, the reflectance spectra of all the polymer films appear very similar to one another, which is in accord with that the reflectance properties of these polymer films appear not to account for the differences in the performance data of the solar cells obtained from these films. However, the marginal 0.2 nm difference in RMS roughness is consistent with the slightly more reflective EMD3 film than EM, with the difference within the margin of experimental errors.

The use of this simple one-step modification is found to greatly improve the longevity of the HSCs. One of the key features of DMSO in PEDOT:PSS solution that is distinctive from EG is the stronger interaction of DMSO with protonated PSS^-.[39] Specifically, the vacuum interaction energy of the DMSO-PSSH complex (−1.22 eV) is more negative than that for the EG-PSSH complex (−1.01 eV). This indicates that the interactions are energetically more favorable for DMSO–PSSH, with a more negative value corresponding to a stronger interaction that leads to a more stable complex. As the primary type of interaction is hydrogen bonding, the oxygen atom in DMSO facilitates unusually strong hydrogen bonding with the –S–O–H moiety in the sulfonic acid group of PSSH (with the hydrogen bond length between PSSH and DMSO being 1.05 Å).[40] Furthermore, as the methyl hydrogens in DMSO interact with the two sulfonate oxygen atoms in PSSH (Fig. 6), this has led to complete coverage of PSSH and reduction in the interactions of the $–SO_3H$ groups in PSSH with other PSS and PEDOT chains. As a result, the excess insulating PSSH shells can be separated from the PSS^- modified $PEDOT^+$.[36,39,40]

DMSO can also cause PSS to aggregate and create pathways for charge movement.[15,33,41,42] This makes the implementation of DMSO as a cosolvent a promising approach to conductivity enhancement. On the other hand, because EG can only provide two strong hydrogen bonds with PSS^-, incorporation of these two cosolvents with different mechanisms together can improve the electrical conductivity of PEDOT:PSS solution. The bond formation of PSSH to DMSO causes rearrangement of the PEDOT chain and improves the phase separation of the PSSH matrix while stabilizing the PSSH matrix. The removal of the insulating PSSH shells that cover the conductive PEDOT moiety enhances the electrical conductivity. Furthermore, it has been reported that methanol has the same phase separation effect and it can also be used to improve the wettability of PEDOT:PSS.[31,43] In the standard form of PEDOT:PSS in electronic applications, PEDOT is the cationic part of the polymer, while PSS is negatively charged. Different pH conditions and local chemical environments during or post fabrication could therefore shift the equilibrium toward more PSSH.[29] Due to the phase separation, PSSH and PEDOT complexes coexist in the solution.[33,44,45] DMSO is an excellent candidate for enhancing the conductivity and stability of PEDOT:PSS due to its strong interaction with the insulating PSSH component. This interaction between DMSO and the sulfonic acid group of PSSH (polystyrene sulfonic acid) is stronger than the interaction between PSS and PSS and that between PEDOT and PSS. This therefore allows DMSO to more effectively remove the insulating PSS shell surrounding the conductive PEDOT chains, enabling the PEDOT chains to aggregate and form a more conductive pathway. The removal or reduction of the PSS shell is a primary route for increasing the electrical conductivity of PEDOT:PSS. The effectiveness of DMSO in removing the PSSH shell can pave the way for a second solvent such as EG, with a different interaction mechanism, to target the remaining PSS chains. This combined approach results in a significant improvement in conductivity compared to employing just DMSO. As the acidity of PEDOT:PSS that leads to its fast degradation is caused by PSS, removal of PSS also protects the electrodes from corrosion and leads to greater stability.[24,46] It

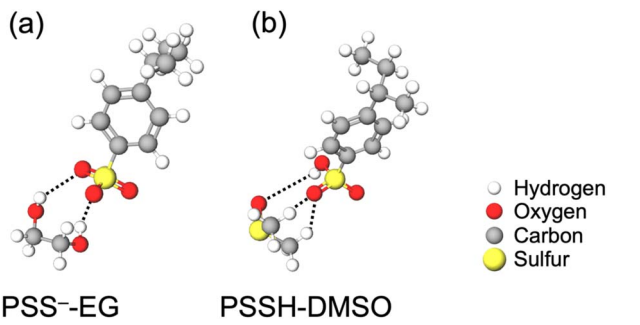

Fig. 6 Schemes of proton sharing between (a) PSS^- and EG and (b) PSSH and DMSO.

should be noted that too high a concentration of cosolvents could counteract the desired effects by acting as insulating materials themselves or introducing cracks into the film.[16,25,34]

In addition, DMSO can enhance the mechanical stability of PEDOT:PSS films, largely due to the structural and morphological changes that DMSO induces within the polymer network. As a secondary dopant that reorganizes the PEDOT structure, DMSO facilitates more effective ordering of PEDOT chains. This organized structure improves crystallinity and results in a denser, more uniform film, which contributes to better mechanical stability along with enhanced electrical conductivity. The most important way that DMSO strengthens mechanical stability is by reducing the amount of PSS, an insulating and relatively brittle component, that covers the PEDOT chains. This reduction decreases the hydrophilic nature of the PEDOT layer, making it less prone to swelling and degradation under humid conditions, which would otherwise reduce the structural integrity of the film. By facilitating PEDOT alignment and its phase separation from PSS, DMSO-treated films can improve flexibility and resistance to crack propagation and to environmental factors, such as humidity and moisture, which are common challenges for PEDOT in electronic applications.[33,47,48]

To date, the highest reported efficiencies for simple planar heterojunction solar cell structures have typically been less than 16%,[20,31,49–54] achieved without the implementation of elaborate techniques such as micro/nano-texturing of the substrate, addition of anti-reflection coatings or passivation layers, and fabrication of more complex perovskite solar cells. Most, if not all, of these processes are generally not cost effective, because they involve the use of more complex procedures and advanced equipment.[55–60] Furthermore, the stability of this type of solar cell in the following days after fabrication is unclear, as it is often not reported in the literature.

The most common approach to enhancing the stability of solar cells is encapsulation. This process involves adding a protective layer to shield the cells from environmental factors such as moisture, oxygen, UV exposure and mechanical damage. Techniques used for encapsulation include spin coating, atomic layer deposition (ALD), plasma-enhanced chemical vapor deposition (PECVD), roll-to-roll printing, screen printing, and lamination.[46,61–65] However, any additional step could introduce complications into the process and increase the cost of fabrication. Techniques such as ALD and PECVD that produce high quality and conformal coatings are expensive and time consuming, especially for large scale production. Additionally, some encapsulation materials may have limited compatibility with specific types of solar cells, particularly organic or organic–inorganic solar cells, where chemical reactions between the encapsulant and active materials could negatively impact performance. Here, we have demonstrated the fabrication of solar cells that are intrinsically more stable by avoiding extra costly steps. In the present work, the sample cells are stored under ambient conditions with no further protection or modification. DMSO incorporated into EM-added PEDOT:PSS is found to have a remarkably positive effect on the stability of these planar heterojunction solar cells.

Conclusions

In this study, the effects of adding DMSO to EM-added PEDOT:PSS solutions used in HSCs have been investigated. Our experiments demonstrate that DMSO can enhance both the electrical conductivity and the longevity of these solar cells. The addition of DMSO to methanol and EG cosolvents facilitates the deposition of a more homogeneous PEDOT:PSS film, improving charge carrier mobility and phase separation of PEDOT and PSS, as DMSO effectively removes the PSS shells and thus improves conductivity and stability. Indeed, the interaction of DMSO with PSSH, which complements that of EG with PSS^-, is particularly beneficial in increasing the PEDOT-to-PSS ratio while retaining the integrity of the film interfaces. The most notable results are obtained with our EMD3 sample, which exhibits minimal efficiency loss (10.6% of its as-fabricated value) 72 h after fabrication, highlighting the potential for achieving more stable solar cells. In contrast, the control sample (EM), with no DMSO added, shows rapid degradation. It is noteworthy that no special care or protection has been applied to these cells while they are stored under ambient conditions. This suggests that the simple addition of DMSO to the existing EG and methanol cosolvents could be the key to improving the stability and performance of PEDOT:PSS-based solar cells, potentially without any need for encapsulation. These findings suggest that the DMSO-EM-PEDOT:PSS approach can be broadly extended to other PEDOT:PSS-based applications, offering a simple strategy for enhancing conductivity and long-term stability across various organic and optoelectronic devices.

Conflicts of interest

There are no conflicts to declare.

Data availability

The data supporting this article have been included as part of the supplementary information (SI). Supplementary information: Tables S1–S5 (performance data of solar cells fabricated with different parameters to illustrate dependence on DMSO concentrations, ambient storage times, sample reproducibility with and without ambient storage, and measurement reproducibility) and Fig. S1 (reflectance data of relevant films used for solar cell fabrication). See DOI: https://doi.org/10.1039/d5ta10078j.

Acknowledgements

This work was supported by the Natural Sciences and Engineering Research Council of Canada.

Notes and references

1 M. Wright and A. Uddin, *Sol. Energy Mater. Sol. Cells*, 2012, **107**, 87–111.

2 T. Zhang, S. Iqbal, X.-Y. Zhang, W. Wu, D. Su and H.-L. Zhou, *Sol. Energy Mater. Sol. Cells*, 2020, **204**, 110245.
3 J. P. Thomas, M. A. Rahman, S. Srivastava, J.-S. Kang, D. McGillivray, M. Abd-Ellah, N. F. Heinig and K. T. Leung, *ACS Nano*, 2018, **12**, 9495–9503.
4 Y. Xia, G. Yan and J. Lin, *Nanomaterials*, 2021, **11**, 3119.
5 S. Khasim, A. Pasha, M. Lakshmi, P. Chellasamy, M. Kadarkarai, A. A. A. Darwish, T. A. Hamdalla, S. A. Al-Ghamdi and S. Alfadhli, *Opt. Mater.*, 2022, **125**, 112109.
6 N. A. Shahrim, Z. Ahmad, A. Wong Azman, Y. Fachmi Buys and N. Sarifuddin, *Mater. Adv.*, 2021, **2**, 7118–7138.
7 Y. Huang, L. Tang and Y. Jiang, *CCS Chem.*, 2024, **6**, 1844–1867.
8 F.-X. Jiang, J.-K. Xu, B.-Y. Lu, Y. Xie, R.-J. Huang and L.-F. Li, *Chin. Phys. Lett.*, 2008, **25**, 2202.
9 S. Khademi, B. Pourabbas and K. Foroutani, *Polym. Bull.*, 2018, **75**, 4291–4309.
10 C. S. Suchand Sangeeth, M. Jaiswal and R. Menon, *J. Phys.: Condens. Matter*, 2009, **21**, 072101.
11 J.-R. Kim, J. H. Jung, W. S. Shin, W.-W. So and S.-J. Moon, *J. Nanosci. Nanotechnol.*, 2011, **11**, 326–330.
12 C. Greco, A. Melnyk, K. Kremer, D. Andrienko and K. Ch. Daoulas, *Macromolecules*, 2019, **52**, 968–981.
13 J. Ouyang, *Displays*, 2013, **34**, 423–436.
14 M. Łapkowski and A. Pron, *Synth. Met.*, 2000, **110**, 79–83.
15 J. P. Thomas, L. Zhao, D. McGillivray and K. Tong Leung, *J. Mater. Chem. A*, 2014, **2**, 2383–2389.
16 S. Mahato, J. Puigdollers, C. Voz, M. Mukhopadhyay, M. Mukherjee and S. Hazra, *Appl. Surf. Sci.*, 2020, **499**, 143967.
17 A. Iyer, J. Hack, D. Angel Trujillo, B. Tew, J. Zide and R. Opila, *Appl. Sci.*, 2018, **8**, 2052.
18 A. Srivastava, R. K. Sharma, D. Sharma, J. S. Tawale, V. V. Agrawal and S. K. Srivastava, *Opt. Mater.*, 2022, **134**, 112922.
19 A. Srivastava, R. K. Sharma, D. Sharma, P. Kumari, V. V. Agrawal and S. K. Srivastava, *Surf. Interfaces*, 2023, **38**, 102822.
20 J. P. Thomas and K. T. Leung, *Adv. Funct. Mater.*, 2014, **24**, 4978–4985.
21 I. Cruz-Cruz, M. Reyes-Reyes, M. A. Aguilar-Frutis, A. G. Rodriguez and R. López-Sandoval, *Synth. Met.*, 2010, **160**, 1501–1506.
22 C. T. Howells, S. Saylan, H. Kim, K. Marbou, T. Aoyama, A. Nakao, M. Uchiyama, I. D. W. Samuel, D.-W. Kim, M. S. Dahlem and P. André, *J. Mater. Chem. A*, 2018, **6**, 16012–16028.
23 M. Jørgensen, K. Norrman, S. A. Gevorgyan, T. Tromholt, B. Andreasen and F. C. Krebs, *Adv. Mater.*, 2012, **24**, 580–612.
24 J. Cameron and P. J. Skabara, *Mater. Horiz.*, 2020, **7**, 1759–1772.
25 S. Zhang, P. Kumar, A. S. Nouas, L. Fontaine, H. Tang and F. Cicoira, *APL Mater.*, 2014, **3**, 014911.
26 J. J. Lee, S. H. Lee, F. S. Kim, H. H. Choi and J. H. Kim, *Org. Electron.*, 2015, **26**, 191–199.
27 Q. Wang, C.-C. Chueh, M. Eslamian and A. K.-Y. Jen, *ACS Appl. Mater. Interfaces*, 2016, **8**, 32068–32076.
28 J. Dong and G. Portale, *Adv. Mater. Interfaces*, 2020, **7**, 2000641.
29 X. Fan, W. Nie, H. Tsai, N. Wang, H. Huang, Y. Cheng, R. Wen, L. Ma, F. Yan and Y. Xia, *Adv. Sci.*, 2019, **6**, 1900813.
30 R. M. Vedovatte, M. C. Saccardo, E. L. Costa and C. E. Cava, *J. Mater. Sci.: Mater. Electron.*, 2020, **31**, 317–323.
31 J. P. Thomas and K. T. Leung, *J. Mater. Chem. A*, 2016, **4**, 17537–17542.
32 Y.-J. Lin, J.-Y. Lee and S.-M. Chen, *Chem. Phys. Lett.*, 2016, **664**, 213–218.
33 I. Lee, G. W. Kim, M. Yang and T.-S. Kim, *ACS Appl. Mater. Interfaces*, 2016, **8**, 302–310.
34 J.-S. Yeo, J.-M. Yun, D.-Y. Kim, S. Park, S.-S. Kim, M.-H. Yoon, T.-W. Kim and S.-I. Na, *ACS Appl. Mater. Interfaces*, 2012, **4**, 2551–2560.
35 X. Crispin, F. L. E. Jakobsson, A. Crispin, P. C. M. Grim, P. Andersson, A. Volodin, C. van Haesendonck, M. Van der Auweraer, W. R. Salaneck and M. Berggren, *Chem. Mater.*, 2006, **18**, 4354–4360.
36 Y. Zhang, Q. Wang, F. Hu, Y. Wang, D. Wu, R. Wang and S. Duhm, *ACS Phys. Chem. Au*, 2023, **3**, 311–319.
37 D. McGillivray, J. P. Thomas, M. Abd-Ellah, N. F. Heinig and K. T. Leung, *ACS Appl. Mater. Interfaces*, 2016, **8**, 34303–34308.
38 B. Peng, X. Guo, C. Cui, Y. Zou, C. Pan and Y. Li, *Appl. Phys. Lett.*, 2011, **98**, 243308.
39 Q. Zhu, E. Yildirim, X. Wang, X. Y. D. Soo, Y. Zheng, T. L. Tan, G. Wu, S.-W. Yang and J. Xu, *Front. Chem.*, 2019, **7**, 783.
40 E. Yildirim, G. Wu, X. Yong, T. L. Tan, Q. Zhu, J. Xu, J. Ouyang, J.-S. Wang and S.-W. Yang, *J. Mater. Chem. C*, 2018, **6**, 5122–5131.
41 L.-M. Yu, T. Chen, N. Feng, R. Wang, T. Sun, Y. Zhou, H. Wang, Y. Yang and Z.-H. Lu, *Sol. RRL*, 2020, **4**, 1900513.
42 M. Pietsch, M. Y. Bashouti and S. Christiansen, *J. Phys. Chem. C*, 2013, **117**, 9049–9055.
43 S. R. S. Kumar, N. Kurra and H. N. Alshareef, *J. Mater. Chem. C*, 2016, **4**, 215–221.
44 Y. H. Kim, C. Sachse, M. L. Machala, C. May, L. Müller-Meskamp and K. Leo, *Adv. Funct. Mater.*, 2011, **21**, 1076–1081.
45 D. A. Mengistie, P.-C. Wang and C.-W. Chu, *J. Mater. Chem. A*, 2013, **1**, 9907–9915.
46 R. K. Sharma, A. Srivastava, U. Punia, R. Bansal, P. Prajapat, G. Gupta and S. K. Srivastava, *Sustainable Energy Fuels*, 2024, **8**, 4799–4812.
47 X. Wang, M. Ge and G. Feng, *Fibers Polym.*, 2015, **16**, 2578–2585.
48 H. Yousefian, A. Babaei-Ghazvini, A. A. Isari, S. A. Hashemi, B. Acharya, A. Ghaffarkhah and M. Arjmand, *Surf. Interfaces*, 2024, **51**, 104481.
49 Q. Ren, J. Qiu, X. Lv, H. Li, L. Yan, C. Meng, Y. Yang and Y. Mai, *ACS Appl. Mater. Interfaces*, 2020, **12**, 25075–25080.
50 Z. Luo, C. Yang, X. Chen, W. Ma, S. Li and K. Fu, *J. Materiomics*, 2023, **9**, 438–446.
51 G. Zhang, H. Peng, Q. Wei, Z. Zhou, H. Wu, J. Luo, J. Wang, X. Wen and Y. Yang, *ACS Omega*, 2024, **9**, 15040–15051.

52 L. Jiang, Z. Zhou, G. Zhang, C. Li, Q. Feng, Q. Wei, J. Li, H. Wu, Y. Shi, J. Wang and Y. Yang, *ACS Appl. Energy Mater.*, 2024, **7**, 3927–3936.
53 J. Chen, Z. Lu, X. Wang, Y. Luo, Y. Ma, G. Lou, D. Chi and S. Huang, *Nanomaterials*, 2024, **14**, 1630.
54 Y. Cui, Y. Xiong, J. Wang, Y. Zhang and W. Yu, *J. Alloys Compd.*, 2025, **1029**, 180782.
55 H.-D. Um, D. Choi, A. Choi, J. H. Seo and K. Seo, *ACS Nano*, 2017, **11**, 6218–6224.
56 Z. Yang, P. Gao, J. He, W. Chen, W.-Y. Yin, Y. Zeng, W. Guo, J. Ye and Y. Cui, *ACS Energy Lett.*, 2017, **2**, 556–562.
57 Y. Han, Y. Liu, J. Yuan, H. Dong, Y. Li, W. Ma, S.-T. Lee and B. Sun, *ACS Nano*, 2017, **11**, 7215–7222.
58 H. Jeong, H. Song, Y. Pak, I. K. Kwon, K. Jo, H. Lee and G. Y. Jung, *Adv. Mater.*, 2014, **26**, 3445–3450.
59 M. Sharma, P. R. Pudasaini, F. Ruiz-Zepeda, D. Elam and A. A. Ayon, *ACS Appl. Mater. Interfaces*, 2014, **6**, 4356–4363.
60 H.-P. Wang, T.-Y. Lin, M.-L. Tsai, W.-C. Tu, M.-Y. Huang, C.-W. Liu, Y.-L. Chueh and J.-H. He, *ACS Nano*, 2014, **8**, 2959–2969.
61 A. Machín and F. Márquez, *Materials*, 2024, **17**, 1165.
62 J. Schmidt, V. Titova and D. Zielke, *Appl. Phys. Lett.*, 2013, **103**, 183901.
63 J. Schmidt, R. Peibst and R. Brendel, *Sol. Energy Mater. Sol. Cells*, 2018, **187**, 39–54.
64 J. He, P. Gao, Z. Yang, J. Yu, W. Yu, Y. Zhang, J. Sheng, J. Ye, J. C. Amine and Y. Cui, *Adv. Mater.*, 2017, **29**, 1606321.
65 S. Ma, G. Yuan, Y. Zhang, N. Yang, Y. Li and Q. Chen, *Energy Environ. Sci.*, 2022, **15**, 13–55.

